Received: 6 May 2022 | Revised: 30 July 2022 | Accepted: 30 July 2022

DOI: 10.1111/jace.18865

Journal of the American Ceramic Society

RESEARCH ARTICLE

$NiMn_2O_4$ revisited: Temperature-dependent cation distribution from in situ neutron diffraction and thermopower studies

Jan Dinger[1] | **Thomas Friedrich**[1,2] | **Timmy Reimann**[1,3] | **Jörg Töpfer**[1]

[1]Department of SciTec, Ernst-Abbe-Hochschule Jena, (Univ. Appl. Sciences Jena), Jena, Germany

[2]EMAT, University of Antwerp, Antwerp, Belgium

[3]INNOVENT e.V. Technologieentwicklung, Jena, Germany

Correspondence
Jörg Töpfer, Department of SciTec, Ernst-Abbe-Hochschule Jena, (Univ. Appl. Sciences Jena), Carl-Zeiss-Promenade 2, 07745 Jena, Germany.
Email: joerg.toepfer@eah-jena.de

Funding information
Thuringian Ministry for Economy, Science and Digital Society—European Social Fund Thuringia, Germany, Grant/Award Number: 2015 FGR 0084

Abstract

The cation distribution of the negative temperature coefficient (NTC) thermistor spinel $NiMn_2O_4$ was studied in the temperature range from 55 to 900°C, using a combined in situ neutron diffraction and thermopower study. Rietveld refinements of in situ neutron diffraction data reveal a temperature dependence of the degree of inversion with an inversion parameter of 0.70(1) at 900°C and 0.87(1) at 55°C. Thermopower measurements were evaluated using a modified Heikes formula, and the $[Mn^{4+}]/[Mn^{3+}]$ ratio on octahedral sites of the spinel structure was calculated considering spin and orbital degeneracy. The inversion degree and disproportionation parameter, determined independently as function of temperature, were used to calculate the cation distribution of $NiMn_2O_4$ in the whole temperature range. At high temperature, within the stability range of the spinel, the cation distribution is characterized by a moderate degree of inversion with a concentration of $Ni_B^{2+} = 0.71(2)$ and small tendency toward disproportionation with a high concentration of $Mn_B^{3+} = 0.98(2)$. At 55°C, cation inversion is enhanced as illustrated by a large concentration of $Ni_B^{2+} = 0.87(2)$, and a small $Mn_B^{3+} = 0.24(2)$ content indicates extensive Mn-disproportionation. Finally, conclusions regarding possible ageing mechanisms of this important NTC thermistor material are drawn.

KEYWORDS
cation distribution, neutron diffraction, NTC thermistors, Seebeck coefficient, spinels, thermoelectric power

1 | INTRODUCTION

Nickel manganite, $NiMn_2O_4$, and similar substituted spinel-type manganese oxides are used for NTC (negative temperature coefficient) thermistor passive devises.[1] Charge transport in these semiconducting oxides takes place via hopping of small polarons, that is, charge carriers (electrons or holes) with their polarized lattice environment, including a thermally activated mobility.[2] The resistivity, ρ, of an oxide thermistor depends on temperature

according to

$$\rho = \rho_\infty \exp\left(\frac{E_a}{k_B T}\right) \quad (1)$$

with ρ_∞ being the resistivity at infinite temperature, k_B is the Boltzmann constant, and E_a is the activation energy for electron transport. Usually, a thermistor constant $B = E_a/k_B$ with typical values of B between 3000 and 4500 K is used, which is proportional to the thermistor's sensitivity. One of the critical issues in NTC thermistors is ageing upon operation, that is, a significant change in resistance with time. This phenomenon is still not completely understood yet, and several ageing mechanisms have been proposed, including: (i) changes in the bulk chemistry, that is, nonequilibrium compositions in the operating temperature range of the thermistor, (ii) temperature-dependent changes in cation distribution, or (iii) partial oxidation and formation of cation-deficient defect spinels.[3–5] For $NiMn_2O_4$, all three scenarios might contribute to ageing. According to the phase diagram $NiO - Mn_2O_3 - O_2$ the spinel $NiMn_2O_4$ is stable in air between 730 and 900°C only.[6] At $T < 730$°C, the spinel is metastable, and long-term annealing of spinel powder was shown to result in partial spinel decomposition and formation of $NiMnO_3$ and $\alpha - Mn_2O_3$.[4,6] Cation-deficient spinels were observed as results of Ni–Mn-oxalate decomposition,[7,8] or as starting products of spinel oxidation.[4] Hence, thermodynamic instability and formation of cation defective spinels with higher cation diffusivities at the operating temperature of the thermistor might contribute to ageing. Moreover, the cation distribution in $NiMn_2O_4$ is complex and varies with temperature; this might also pose a potential risk of changing charge carrier concentrations with time upon operational conditions of the thermistor.

The spinel structure is characterized by a cubic close packaging (ccp) of oxygen ions. Cations occupy tetrahedral 8*a* sites (A-sites) and octahedral 16*d* sites (B-sites), and one half of the octahedral and one eighth of the tetrahedral positions are occupied. Oxygen ions reside on 32*e* positions with the oxygen *u*-parameter. The unit cell consists of eight formula units.[9] The distribution of cations between A and B-sites is governed by two main factors. The degree of inversion ν, describing the exchange of nickel and manganese ions among tetrahedral and octahedral sites, is dominated by the large octahedral crystal field stabilization of Ni^{2+} ions.[10] Second, a distinct tendency toward the disproportionation of $2Mn_B^{3+} \rightleftarrows Mn_A^{2+} + Mn_B^{4+}$ is present, causing $NiMn_2O_4$ to be a cubic and mostly inverse spinel, unlike other tetragonal and normal manganese spinels $A[Mn_2]O_4$ with A = Mg,[11] Mn,[12] and Zn.[13] Many studies devoted to the determination of the cation distribution of $NiMn_2O_4$ were performed in the last 60 years. Baltzer[14] and Sinha et al.[10] estimated an inverse cation distribution $Mn^{2+}[Ni^{2+}Mn^{4+}]O_4$ (octahedral position denoted by brackets) using X-ray diffraction (XRD) and magnetic measurements. Boucher et al. derived a partially inverse distribution $Ni^{2+}_{1-\nu}Mn^{3+}_{\nu}[Ni^{2+}_{\nu}Mn^{3+}_{2-\nu}]O_4$ from neutron diffraction experiments with a temperature-dependent degree of inversion, for example, with $\nu = 0.74$ for quenched and $\nu = 0.93$ for slow cooled samples.[15] Larson et al.[16] assumed the cation distribution as $Mn^{2+}_{0.65}Mn^{3+}_{0.35}[Ni^{2+}Mn^{3+}_{0.35}Mn^{4+}_{0.65}]O^{2-}_4$ using combined XRD, electrical, magnetic, and Seebeck measurements. In the following years, many studies using different experimental techniques demonstrated that the cation inversion is coupled with manganese disproportionation, as described by the general formula:

$$Ni^{2+}_{1-\nu}Mn^{3+}_{\nu-p}Mn^{2+}_{p}\left[Ni^{2+}_{\nu}Mn^{3+}_{2-\nu-p}Mn^{4+}_{p}\right]O_4 \quad (2)$$

with the degree of inversion ν and the disproportionation parameter p. Using photoelectron spectroscopy, cation distributions with large inversion degrees of $\nu = p = 0.90$ were confirmed.[17,18] From room-temperature neutron diffraction studies, Gillot et al. found a $\nu = 0.88$ and $p = 0.78$;[19] Sagua et al.[20] reported a $\nu = 0.79$. Thermopower (Seebeck coefficient) measurements showed an $S = -110\ \mu$V/K near room-temperature signaling n-type electron charge transport, and a cation distribution with $\nu = p = 0.85$ was derived using Heikes formula.[21]

Most studies extracted cation distributions from diffraction data, spectra, or physical properties measured at room temperature, and considerable scattering of the results is observed in the literature. This is caused by the fact that the cation distribution depends on temperature (see, e.g., Ref. [15]), and therefore, the thermal history of the samples, that is, sintering temperature, dwell time, and cooling rates might affect the results of ex situ characterization studies. Reports on in situ monitoring of the temperature-dependent cation distribution in $NiMn_2O_4$ are scarce. Measurements of the thermopower (Seebeck coefficient S) of $NiMn_2O_4$ between 100 and 600°C have revealed a change in activation energy at about 400°C, which was interpreted as onset of cation redistribution processes.[22] Recently, a decrease of the absolute Seebeck coefficient of $NiMn_2O_4$ with temperature, and even a change of sign to p-type at about 770°C was observed.[23] This prompted us to perform thermopower measurements of samples with different thermal histories from room temperature up to about 900°C, that is, the upper temperature stability limit of $NiMn_2O_4$.[24] Using the modified Heikes formula, and including electron degeneracies, we suggested cation distributions for a wide temperature range. However, as Heikes formula allows to calculate

the ratio $[Mn_B^{4+}]/[Mn_B^{3+}]$ and therefore allows to monitor the Mn-disproportionation equilibrium only, we were not able to unequivocally determine temperature-dependent cation distributions of $NiMn_2O_4$ based on thermopower measurements alone.[24]

In this study, we report for the first time about in situ neutron diffraction and thermopower measurements in the range from near room temperature up to 900°C. The degree of inversion ν was obtained from Rietveld refinements of neutron diffraction data, and the $[Mn_B^{4+}]/[Mn_B^{3+}]$ ratio and the Mn-disproportionation parameter p were calculated from the analysis of the Seebeck coefficients. From the combination of both data sets, we propose a cation distribution model of $NiMn_2O_4$ for temperatures from 55 up to 900°C. This might add new arguments to the discussion, whether or not and which of the different mechanisms contribute to the ageing of resistance with time under operational temperature conditions of the $NiMn_2O_4$ thermistors.

2 | MATERIALS AND METHODS

2.1 | Sample preparation

Samples of $NiMn_2O_4$ were prepared using the oxalate precursor route. Mn-II-acetate and $NiCO_3$ were dissolved in an acetic acid solution. The exact metal contents of the Mn and Ni starting materials were precisely determined by thermogravimetric analysis through annealing in Pt crucibles at 1200 and 800°C, respectively, and the obtained factors were used for weighing stoichiometric amounts of both ingredients. A slight excess of oxalic acid solution was added to precipitate the oxalates at room temperature. The mixed oxalate powder was thermally decomposed by annealing for 5 h at 350°C. Pellets of the resulting oxide powder were fabricated by uniaxial pressing. All samples were sintered in a tube furnace at 1150°C for 1 h in oxygen atmosphere. To obtain a single-phase spinel, the pellets were reoxidized for 40 h at 850°C in air. Finally, the samples were equilibrated at 900°C in air for 20 h and slowly cooled with 5 K/min (SC900). One sample set for Seebeck measurements was equilibrated at 800°C in air for 20 h and quenched in water (Q800).

2.2 | Measurements

The BET specific surface area (SSA) was determined using a Nova 3200e Quantachrome analyzer. According to $d_{BET} = 6/(\rho\ SSA)$, the particle size d_{BET} was calculated using the theoretical density ρ obtained from the lattice parameters assuming spherical particles. The Mn average oxidation state was determined using redox titrations by dissolving the samples in an excess of 0.1 N VO^{2+} solution and titration with 0.1 N $KMnO_4$ solution. According to the formula, $Ni^{2+}Mn_2^{2+k}O_{3+k}$ (with k as redox equivalent) values of $k = 1$ indicate the formation of a single spinel phase with an average Mn oxidation state of +3.00, whereas a $k < 1$ or $k > 1$ suggests the formation of multiphase mixtures, or defect spinels, respectively.

The phase composition of the samples was studied using XRD (Cu K_α radiation) with a Bruker D8 Advance diffractometer (Bruker AXS, Karlsruhe, Germany) equipped with a LYNXEYE detector. For high-temperature XRD measurements in air, a TC-basic heating stage (MRI, Karlsruhe, Germany) was used. The samples were heated to 860°C (stability area of $NiMn_2O_4$[6]), and measurements were performed during cooling from 860°C to room temperature in adequate steps between the measurements. At each temperature, the data were collected scanning a 2θ range from 17.5° to 91° using a step size of 0.015° and 1 s per step. Neutron Diffraction experiments were performed at the BER II reactor Berlin, Germany, using instrument E9—fine resolution powder diffractometer.[25] The used wavelength was aligned using a Ge-monochromator (Ge-511, $\lambda = 1.7995$ Å). Pellets of $NiMn_2O_4$ were stacked in a quartz tube, which was flushed with air during the measurement. The samples were heated up to 900°C, and measurements were performed during cooling from 900 to 500°C in steps of 50 K between the measurements, or of 100 K at $T < 500$°C. The data were collected using eight area detectors (DENEX ^{3}He 2D, 300 mm × 300 mm) in the range of $3° < 2\theta < 142°$ with a step size of 0.075° 2θ. The measurement time was 4 h to reach a sum of more than 2 million counts. Rietveld refinements of the diffraction data were performed using TOPAS Version 6 (Bruker AXS). The Seebeck coefficient S was measured with a Linseis LSR-3 (Linseis Messgeräte GmbH, Selb, Germany) between 100 and 860°C during heating and cooling with a rate of 1 K/min. Values of the Seebeck coefficient were calculated using the linear regression of nine measurements at the same temperature with different temperature gradients. Seebeck coefficients in the temperature ranges 55–100 and 860–900°C were extrapolated.

3 | RESULTS

3.1 | Sample synthesis

Thermal decomposition of the Ni/Mn-oxalate precursor at 350°C results in nanosized cubic defect spinel powder[8] with large specific area of 270 m^2/g (corresponding to a particle diameter of about $d_{BET} = 5$ nm). Pellets of that

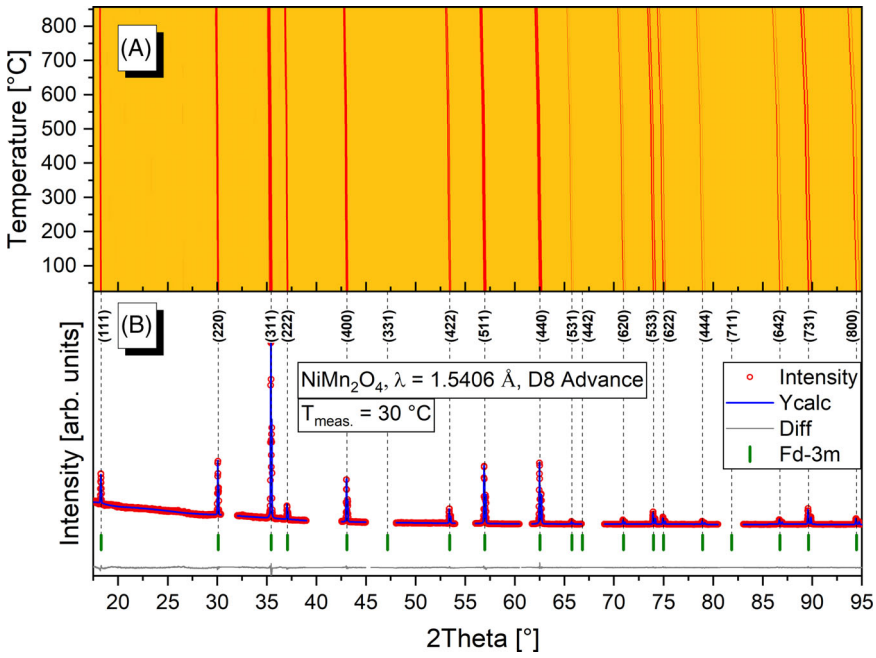

FIGURE 1 X-ray diffraction (XRD) patterns of $NiMn_2O_4$: (A) from room temperature to 860°C as contour plot, (B) Rietveld refinement of an XRD pattern obtained at 30°C

powder were sintered at 1150°C in oxygen (above the upper stability limit of $NiMn_2O_4$ at 1100°C in oxygen, or at 900°C in air [6]). Thus, a partial spinel decomposition upon formation of a Mn-rich spinel and NiO with loss of oxygen according to

$$NiMn_2O_4 \rightleftarrows xNiO + \frac{(3-x)}{3}Ni_{\frac{(3-3x)}{(3-x)}}Mn_{\frac{6}{(3-x)}}O_4 + \frac{x}{6}O_2 \quad (3)$$

takes place.[26] Annealing at 850°C for several hours is required for complete reoxidation and reformation of a single spinel phase in reversal of Equation (3).[27] During the last anneal at 900°C, the cation distribution was equilibrated, and the samples were slowly cooled. The bulk samples have densities of >92%. Measurements of the redox equivalents using chemical titration resulted in values of $k = 0.998(2)$, suggesting that the samples represent single-phase spinels $NiMn_2O_{4.00}$ with an average Mn oxidation state of +3.00.

3.2 | X-ray diffraction measurements

The XRD patterns of $NiMn_2O_4$ measured in situ in the temperature range from 860°C to room temperature are shown in Figure 1A. A single-phase spinel is observed throughout the whole temperature range. As an example, the Rietveld refinement of a diffraction pattern measured at 30°C in space group no. 227 (*Fd*-3*m*) is shown in Figure 1B (background peaks from Pt/Rh sample holder are removed). We have to keep in mind that according to the phase diagram,[6] $NiMn_2O_4$ is unstable at $T < 730$°C in air and transforms into a mixture of ilmenite-type $NiMnO_3$ and bixbyite $\alpha - Mn_2O_3$:

$$NiMn_2O_4 + \frac{1}{4}O_2 \rightleftarrows NiMnO_3 + \frac{1}{2}Mn_2O_3 \quad (4)$$

Decomposition of the spinel in that temperature range was indeed observed after the annealing of spinel powders with high surface area.[27] On the other hand, decomposition of bulk samples during cooling is kinetically impeded, and a metastable cubic $NiMn_2O_4$ spinel is observed at room temperature with its specific cation distribution equilibria adjusted by the annealing and cooling history.

3.3 | Neutron diffraction measurements

The neutron diffraction patterns of $NiMn_2O_4$ obtained at temperatures between 900 and 50°C are shown in Figure 2. The patterns show peaks typical of a spinel lattice with some reflexes having temperature-dependent intensities. Additionally, some lattice planes (hkl) do not exhibit peaks because the different signs of the neutron scattering lengths (Ni = 10.3 fm, Mn = −3.73 fm) cause extinction of these reflections.[28] In contrast to XRD, the lattice planes (220) and (311) are not observed over the whole temperature range. The (331) reflection only appears between 600 and 900°C, whereas (422) is present between 55 and 500°C (Figure 2A).

Rietveld refinements of the neutron diffraction data were performed using a structural model with space group *Fd*-3*m* (Figure 2B), and lattice parameters, oxygen

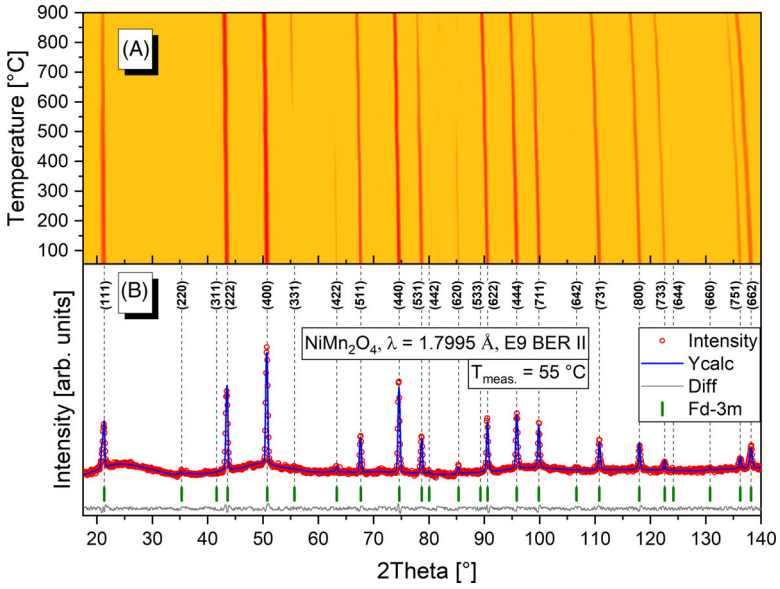

FIGURE 2 Neutron diffraction patterns of $NiMn_2O_4$: (A) from 50 to 900°C as contour plot, (B) Rietveld refinement of a neutron diffraction pattern obtained at 55°C

TABLE 1 Results from Rietveld refinement of the neutron diffraction data

T (°C)	Lattice parameter a_0 (Å)	Oxygen position u (–)	Degree of inversion ν (–)	R_{WP} (%)
55	8.3963 (30)	0.3881 (3)	0.866 (5)	4.67
108	8.3995 (30)	0.3882 (3)	0.865 (5)	3.98
202	8.4052 (30)	0.3882 (3)	0.867 (5)	3.92
300	8.4121 (33)	0.3882 (3)	0.867 (5)	3.83
401	8.4201 (33)	0.3882 (3)	0.854 (5)	3.88
500	8.4285 (36)	0.3881 (3)	0.818 (6)	3.51
551	8.4348 (39)	0.3880 (3)	0.794 (6)	3.58
600	8.4389 (42)	0.3880 (3)	0.781 (7)	3.61
650	8.4432 (39)	0.3877 (3)	0.757 (7)	3.59
700	8.4471 (42)	0.3878 (3)	0.737 (7)	3.47
749	8.4504 (42)	0.3876 (4)	0.722 (8)	3.18
800	8.4573 (45)	0.3875 (4)	0.711 (8)	3.31
850	8.4644 (45)	0.3869 (4)	0.707 (7)	3.39
900	8.4728 (45)	0.3865 (4)	0.703 (7)	3.26

Note: R_{WP}—weighted profile residual.

u-parameters, and site occupancies were obtained (Table 1). From a simple cation distribution model, allowing for the inversion of Ni- and Mn-ions between A- and B-sites of the spinel lattice (without considering cation charges and Mn-disproportionation), the degree of inversion ν was obtained from site occupancies.

3.4 | Seebeck coefficient measurements

The Seebeck coefficient S of $NiMn_2O_4$ is shown as function of temperature in Figure 3. A thermopower of $S = -173\ \mu V/K$ is found at 108°C for the slow cooled sample (SC900), indicating that electrons represent the majority charge carriers at low and intermediate temperatures. The absolute values of the S decrease continuously on heating, and a crossover from negative to positive sign is observed at 680°C. At temperatures above 800°C, the Seebeck coefficient seems to saturate and becomes temperature independent. At $T = 860$°C, an $S = +20\ \mu V/K$ is measured, which is in agreement with results from Ref. [23]. The $S(T)$ characteristic is reversible during the heating/cooling measurements (Figure 3). This is an indication that the slow cooling of $NiMn_2O_4$ obtained via the reported synthesis protocol results in a cation distribution state, which is close to equilibrium, both in the metastable (room temperature up to 730°C) and in the thermodynamically stable range of $NiMn_2O_4$ (730–900°C). Recently, we have

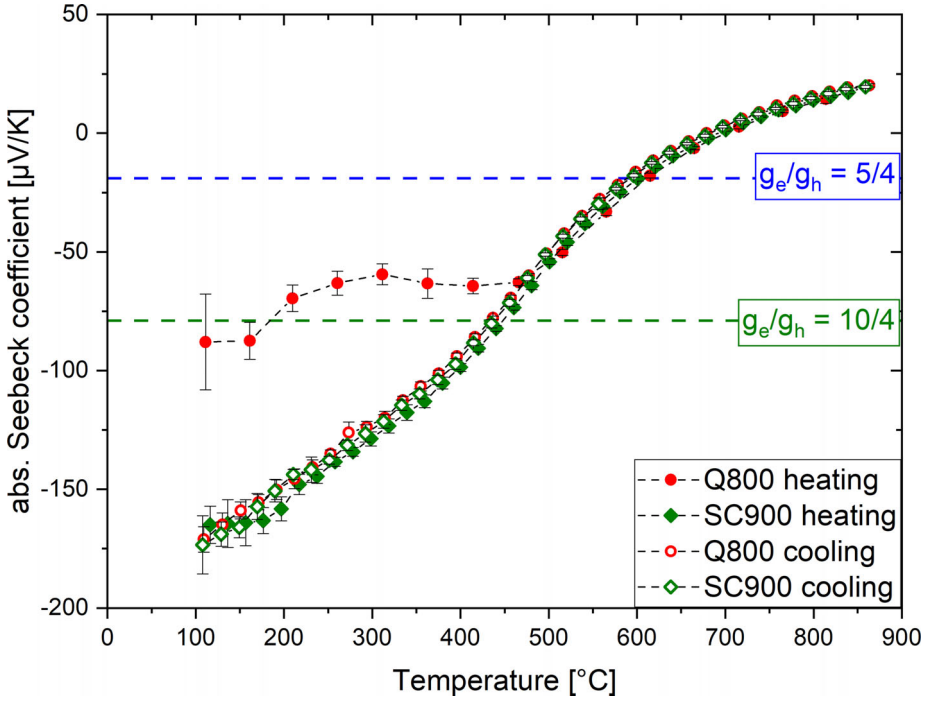

FIGURE 3 Seebeck coefficient of $NiMn_2O_4$ from 100 to 860°C measured on heating and cooling on samples slow cooled from 900°C (SC900) and quenched from 800°C (Q800); horizontal dotted lines represent Seebeck coefficients for $[Mn_B^{4+}]/[Mn_B^{3+}] = 1$ and degeneracy ratios of 5/4 and 10/4.

investigated the thermopower of quenched and slowly cooled samples.[24] It was shown that quenched samples exhibit different room-temperature Seebeck coefficients as compared to slow cooled samples. The variation of the Seebeck coefficient $S(T)$ of a sample quenched from 800°C (Q800) is included in Figure 3. At 108°C, an $S = -88\ \mu V/K$ is observed. On further heating the $S(T)$ curve of the Q800 sample starts to coincide with that of SC900 at about 400°C. Upon further heating to 860°C and on cooling the Seebeck coefficients of both samples are almost identical. This observation suggests that quenching does not allow to freeze-in a high-temperature equilibrium cation Mn-disproportionation state, but rather results in an intermediate nonequilibrium state, different from the cation and Mn-valence distribution obtained after slow cooling. Therefore, in situ high-temperature thermopower measurements are needed to derive information on the equilibrium cation occupation situation.[24] For further analysis, Seebeck coefficients recorded during the cooling run were used to ensure a comparable temperature influence with respect to the neutron diffraction experiment.

4 | DISCUSSION

The cubic lattice parameters a_0 were refined as the function of temperature from both in situ XRD and in situ neutron diffraction measurements with nearly identical results (Figure 4). The lattice parameter increases almost linearly with temperature, starting from $a_0 = 8.3963(24)$ Å at $T = 55$°C and reaching $a_0 = 8.4728(33)$ Å at 900°C (Table 1, Figure 4). Room-temperature lattice parameters reported in the literature scatter to large extend from about $a_0 = 8.380$–8.403 Å,[7,8,15,19–21,29–34] which might originate from the fact that samples were prepared using different synthesis techniques and with different (often not reported in detail) thermal histories. As we have demonstrated recently using XRD,[24] the room-temperature lattice parameter of $NiMn_2O_4$ of quenched samples is very close to that of a slowly cooled sample ($a_0 = 8.3935(3)$ Å, Ref. [24]), with a slight increase with higher quenching temperatures (e.g., $a_0 = 8.3978(4)$ Å, quenched from 850°C,[24]). To the best of our knowledge, there exist no in situ high-temperature data on the crystal structure of $NiMn_2O_4$. It is interesting to note that the lattice parameters a_0 at $T > 800$°C slightly deviate from the almost linear temperature variation (Figure 4, discussion: see later).

In regular cubic spinels (space group *Fd*-3*m*; standard choice of the unit cell origin with point symmetry $\bar{4}3m$ on an A-site cation position), the oxygen ions reside on 32*e* positions, which are no specific positions, but are rather described by the oxygen parameter u. For an ideal spinel with perfect ccp arrangement, the oxygen parameter is $u = 0.375$. For larger oxygen parameters u, the anions move away from the tetrahedral A-cations leading to an increase of tetrahedral site and a reduction in octahedral B-site

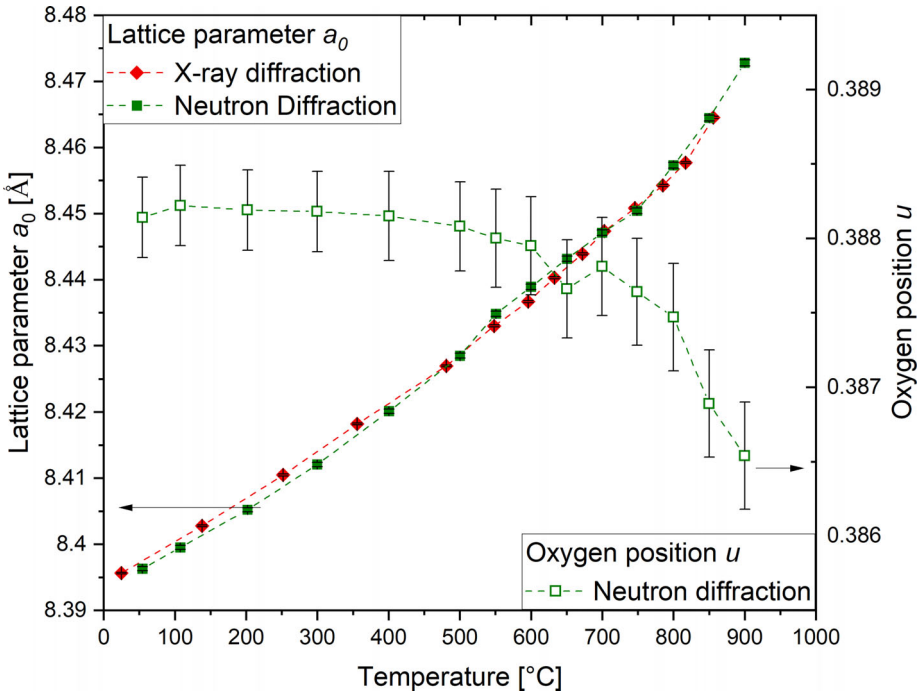

FIGURE 4 Lattice parameter a_0 (from XRD and ND) and oxygen position parameter u (from ND) of $NiMn_2O_4$ versus temperature

volumina.[9] The oxygen parameters were refined from neutron diffraction measurements with values of $R_{wp} < 5\%$. Large oxygen position parameters u are found (Table 1), which decrease slightly from $u = 0.3881(3)$ at 50°C to $u = 0.3875(4)$ at 800°C (Figure 4). At $T > 800$°C, a steeper decline down to $u = 0.3865(4)$ at 900°C is observed. Similar room-temperature values of u were reported.[15,29] Boucher et al. also observed this abrupt decrease of u at $T > 800$°C to 0.3870 at 940°C.[15] It should be stressed again that their measurements were performed on quenched samples at room temperature.

The ability of neutron diffraction to distinguish between cations with similar atomic numbers allows to derive the occupation of Ni and Mn ions on tetrahedral 8*a* (A)- and octahedral 16*d* (B)-positions, and hence, the degree of inversion ν of the spinel (Table 1). At 55°C, a degree of inversion of $\nu = 0.87(1)$ is observed, which remains almost constant up to $T = 300$°C (Figure 5). On further increasing the temperature, ν decreases and reaches $\nu = 0.71(1)$ at 800°C. Up to the upper temperature limit of the measurements at 900°C (i.e., in the stability region of $NiMn_2O_4$[6]), no further change in the degree of inversion takes place. These results confirm the findings of other neutron diffraction studies on $NiMn_2O_4$ reported so far. A similar variation of ν with temperature was reported by Boucher et al.[15] with values of the inversion degree between $\nu = 0.93$ (sample slowly cooled down to room temperature) and $\nu = 0.74$ (sample quenched from 940°C in water). Gillot et al. found $\nu = 0.88$[19] and Sagua et al. reported a $\nu = 0.80$,[20] both studies were performed on slowly cooled samples, measured at room temperature. For the first time, we present the inversion degree of $NiMn_2O_4$ as the function of temperature, derived from in situ neutron diffraction experiments (Figure 5). The good consistency between our data and the results of Boucher et al.[15] indicates that proper quenching of samples is capable of freezing in the corresponding high-temperature cation distribution between tetrahedral and octahedral sites of the spinel lattice. However, neutron diffraction allows to differentiate between Ni and Mn cations without information on charges, and an average Mn oxidation state of Mn^{3+} is assumed expressed by the simple cation distribution model $Ni^{2+}_{1-\nu}Mn^{3+}_{\nu}[Ni^{2+}_{\nu}Mn^{3+}_{2-\nu}]O_4$.[15] At low temperature (between 55 and 300°C), $NiMn_2O_4$ exhibits a large degree of inversion ($\nu = 0.87$) corresponding to an almost inverse spinel. At high temperatures (between 800 and 900°C), that is, in the stability region of the spinel, the inversion is $\nu = 0.71$, which is close to a random configuration of the cations as favored at high temperatures.[35]

The variation of the lattice parameter a_0 and oxygen positional parameter u with the degree of inversion ν is shown in Figure 6. For intermediate values of the inversion degree ν of about 0.72 up to 0.86, a continuous increase of the oxygen parameter u and a decrease of a_0 (reduction of unit cell length with decreasing temperature) are observed. For small inversion parameters of $\nu \cong 0.71$ (i.e., at high temperatures), however, a significant increase in u and a simultaneous drop in a_0 are observed for small variations in ν. As at $T \geq 800$°C the degree of inversion ν is almost constant (Figure 5), the observed changes in a_0

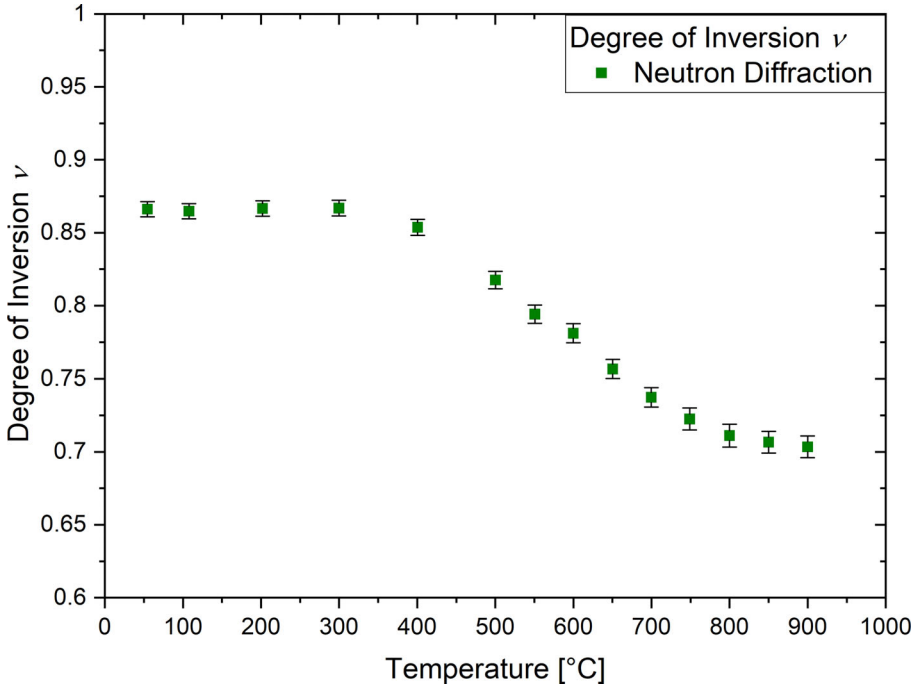

FIGURE 5 Degree of inversion ν of $NiMn_2O_4$ versus temperature obtained from Rietveld refinement of in situ neutron powder diffraction measurements

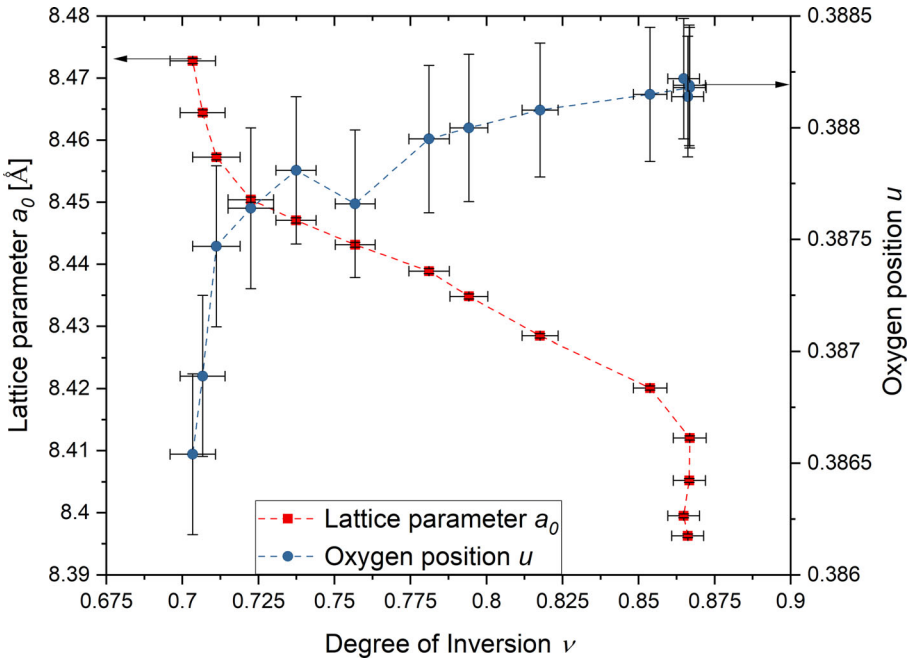

FIGURE 6 Lattice parameter a_0 and oxygen position u as function of degree of inversion ν

and u might point at changes in the Mn-disproportionation equilibrium $2Mn_B^{3+} \rightleftarrows Mn_A^{2+} + Mn_B^{4+}$. With the ionic radii of 0.645 Å for Mn_B^{3+}, 0.66 Å for Mn_A^{2+}, and 0.53 Å for Mn_B^{4+},[36] respectively, a shift of the Mn-disproportionation equilibrium to the right-hand side at nearly constant inversion ν is consistent with a decrease of the lattice parameter. Simultaneously, a slight increase of tetrahedral site and a reduction in octahedral B-site volumina (higher concentrations of Mn_A^{2+} and Mn_B^{4+}) correspond to the observed increase in the oxygen parameter u. Similarly, a strong variation of a_0 and u is found at low temperatures of $T \leq 400°C$ with corresponding large inversion parameters of $\nu = 0.86$–0.87, where due to low kinetics cation exchange between A- and B-sites hardly occurs, but Mn-disproportionation

continues giving rise to a considerable reduction of cell volume. The variation of the Mn-disproportionation equilibrium (experimentally accessed through thermopower measurements) with temperature and inversion will be discussed later.

For oxides with charge transport via hopping of small polarons, Heikes formula is used to describe the Seebeck coefficient in the high-temperature limit[37]:

$$S = -\frac{k_B}{e}\left[\frac{S_T}{k} + \ln\left(\frac{1-c}{c}\right)\right] \quad (5)$$

with $c = n/N$, where N denotes the number of available sites, and n is the number of charge carriers. The entropy of transport S_T/k is small and may be neglected.[38] For electrons with spin $S = 1/2$, the spin degeneracy is to be considered, and a degeneracy factor β was proposed by Chaikin and Beni[39]:

$$S = -\frac{k_B}{e}\left[ln\left(\beta\frac{1-c}{c}\right)\right] \quad (6)$$

As discussed by Doumerc,[40] in a mixed-valency cation system the degeneracy factor β has to take into account the spin degeneracies of all cations taking part in the charge hopping process, and a spin degeneracy of $\beta = \frac{2S_n+1}{2S_{n+1}+1}$ was suggested with the total spins of cations M^{n+} and $M^{(n+1)+}$, respectively. Recently, it was concluded that the orbital degeneracy of the ions involved in the hopping process as well as their crystallographic environment, and crystal field splitting has to be considered well.[41] Koshibae et al. emphasized the effect of the number of configurations g_i of i ions to the Seebeck coefficient[42–44]

$$S = -\frac{k_B}{e}\left[ln\left(\frac{g_e}{g_h}\frac{1-c}{c}\right)\right] \quad (7)$$

with g_e and g_h as electronic degeneracies of the cations acting as electron donors e (e.g., Co^{3+} and Mn^{3+}) or electron acceptors h (holes, Co^{4+}, Mn^{4+}), respectively. Both spin and orbital degeneracies (g_{spin},g_{orbit}) are included in the electronic degeneracy g.

In manganite spinels, electronic conduction is governed by the hopping of charge carriers between Mn^{3+} and Mn^{4+} on octahedral B-sites, and the term $(1-c)/c$ in Equation (7) is equivalent with the ratio $[Mn_B^{4+}]/[Mn_B^{3+}]$. In $NiMn_2O_4$, ferrimagnetic ordering appears below $T_N = 90$ K.[45] As the thermopower measurements were performed at higher temperatures, appropriate electronic degeneracies g_e/g_h should be considered. High-spin states are assumed for the electronic configurations of Mn-ions, and the resulting degeneracies are shown in Figure 7 (inset). In addition, dynamic or static distortions of Jahn–Teller-(JT)-active ions might contribute to the absolute Seebeck coefficient[44] and for JT-active Mn^{3+} ions two different configurations are to be discussed. A total degeneracy of $g = 10$ results for a high-spin Mn_B^{3+} t^3e^1 configuration. If the orbital degeneracy is lifted by the JT effect of Mn_B^{3+}, the total degeneracy is $g = 5$. It has been reported for manganese spinels that cooperative distortions of the spinel lattice with lowering of symmetry occur, if the concentration of JT-active Mn^{3+} ions on B-sites exceeds a critical limit of about 55%–65% of the B-site Mn ions.[46–49] However, on local scale, the JT effect of the Mn_B^{3+} ions might be effective lifting the orbital degeneracy and giving rise to a total degeneracy of $g_e/g_h = 5/4$. On the other hand, if the orbital degeneracy is maintained, a total degeneracy of $g_e/g_h = 10/4$ is expected.

The difference in the Seebeck coefficients at 100°C observed between the quenched sample Q800 and the slowly cooled SC900 sample (Figure 3) is due to different cation distributions and Mn-disproportionation states. The slowly cooled sample with a high degree of inversion ν represents a low-temperature equilibrium Mn-disproportionation state. The sample Q800 has an inversion degree ν of about 0.7 characteristic for high temperatures, as cation exchange between A- and B-site does not seem to take place during quenching. This is supported by the agreement of neutron diffraction results from in situ experiments (Figure 5) and on quenched samples.[15] On the other hand, rapid exchange of electrons between Mn-ions during quenching seems to emerge into a final situation with equal Mn^{3+} and Mn^{4+} concentrations on B-sites. For such scenario, an $S = -79$ μV/K is expected for an electronic degeneracy of $g_e/g_h = 10/4$ and $S = -19$ μV/K for $g_e/g_h = 5/4$, respectively. Experimentally, an $S = -88$ μV/K is observed at 108°C for the quenched sample, indicating that the electronic degeneracy of Mn^{3+} is $g = 10$ without lifting the orbital degeneracy of the t_{2g} and e_g states. Such rapid electron transfer governs the electronic configurations in the spinel Fe_3O_4 as demonstrated using temperature-dependent thermopower measurements.[38] In magnetite electron transfer between Fe^{2+} and Fe^{3+} adjusts the cation inversion equilibrium, and an inverse distribution with equal concentrations of Fe_B^{3+} and Fe_B^{2+} is reached at low temperature. This is similar to the situation in the quenched sample Q800, where cation exchange between A- and B-sites does not take place (as shown with neutron diffraction), and the electron transfer among Mn_B^{3+}, Mn_B^{4+}, and Mn_A^{2+} seems to coincide upon quenching in a situation with equal concentrations of Mn_B^{3+} and Mn_B^{4+}. For hausmannite Mn_3O_4, it was demonstrated that in the stability range of the cubic high-temperature spinel phase between 1175 up to 1500°C a statistical distribution with equal concentrations of Mn_B^{2+}, Mn_B^{3+}, and Mn_B^{4+} exists.[50] Kobayashi also demonstrated

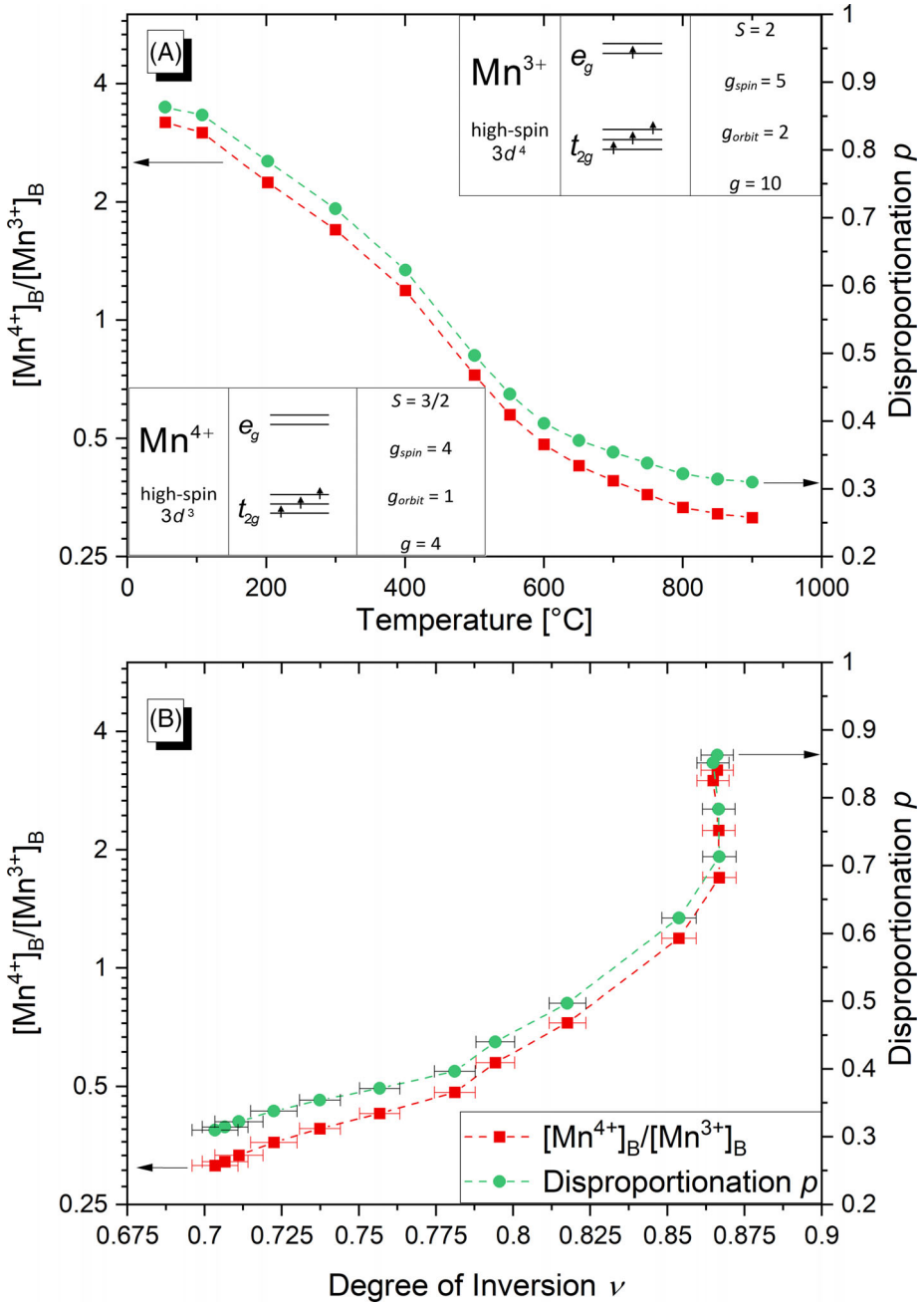

FIGURE 7 $[Mn_B^{4+}]/[Mn_B^{3+}]$ ratio and Mn-disproportionation parameter p as function of (A) temperature and of (B) degree of inversion for $NiMn_2O_4$ (inset in (A): electronic configurations and degeneracies of Mn^{3+} and Mn^{4+} ions)

that for mixed valence Mn^{3+}/Mn^{4+} oxide systems, an electronic degeneracy of $g_e/g_h = 10/4$ without lifting of the orbital degeneracy of octahedral Mn^{3+} is approached at high temperatures.[44]

The ratio of $[Mn_B^{4+}]/[Mn_B^{3+}]$ versus temperature was calculated from the Seebeck coefficients S (Figure 3) using Equation (7) with an electronic degeneracy g_e/g_h of 10/4 (Figure 7). The $[Mn_B^{4+}]/[Mn_B^{3+}]$ ratio decreases almost linearly with temperature between 100 and 300°C (Figure 7A). Above that temperature, a steeper decrease occurs, turning again into a smaller slope in the temperature range from 700 to 860°C. This implies three different regimes of Mn-disproportionation reactions occurring in the whole studied temperature range. The disproportionation parameter p was obtained from the cation distribution model (formula (2)) with $[Mn_B^{4+}]/[Mn_B^{3+}] = p/(2-\nu-p)$. The calculated Mn-disproportionation parameter p is also shown versus temperature in Figure 7. At 100°C we observe a high degree of Mn-disproportionation of $p = 0.85(3)$ dropping to $p = 0.71(1)$ at 300°C (Figure 7). At 850°C, a $p = 0.31(1)$ is consistent with a large concentration of $Mn_B^{3+} = 0.98(1)$. The Mn^{3+} concentration

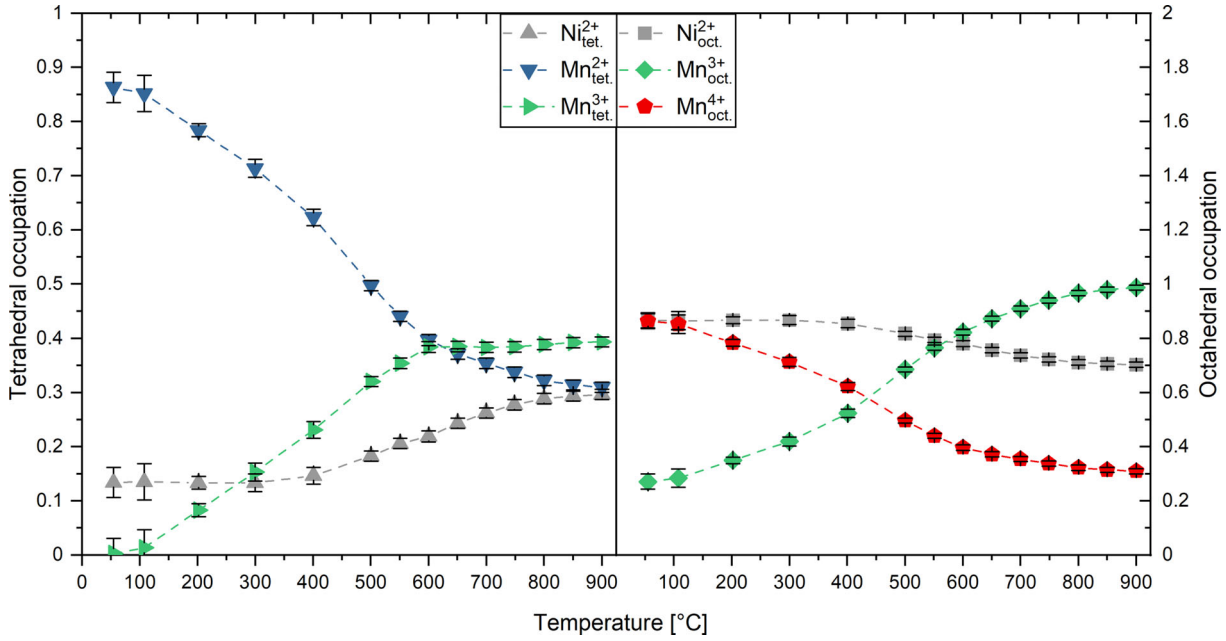

FIGURE 8 Cation distribution of $NiMn_2O_4$ as function of temperature

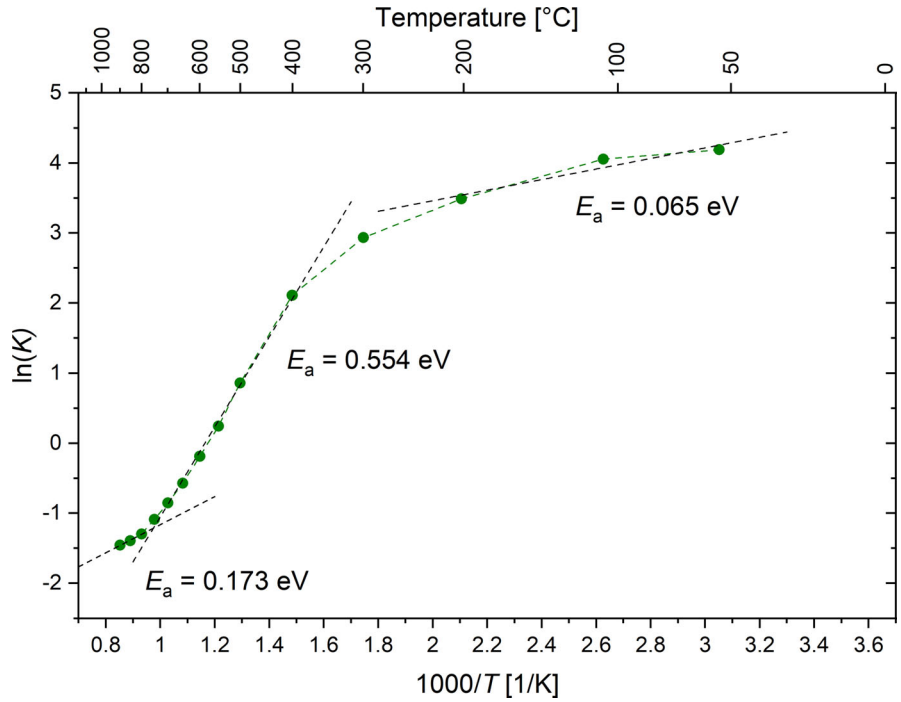

FIGURE 9 Equilibrium constant ln(K) as a function of $1/T$ for $NiMn_2O_4$

on octahedral B-sites (49% of octahedral Mn ions) is still too low to cause cooperative JT distortions and formation of a tetragonal spinel with lower symmetry. The $[Mn_B^{4+}]/[Mn_B^{3+}]$ ratio and p are also depicted as function of the inversion parameter ν (Figure 7B). A general trend of in increasing p with increasing inversion ν (decreasing temperature) is observed. At large values of $\nu > 0.86$, the Mn-disproportionation p increases significantly with ν remaining more or less constant. In that region (with almost constant inversion parameter ν) the Mn-disproportionation increases with decreasing temperature resulting in a high concentration of Mn_A^{2+} and Mn_B^{4+} at room temperature. This is also consistent with the observed decrease of the unit cell parameter in that range of constant ν and decreasing temperature (Figure 6).

The complete cation distribution of $NiMn_2O_4$ was calculated as a function of temperature using the cation distribution model (formula (2)). The degree of inversion ν (Figure 5) was determined by Rietveld refinements of the in situ neutron powder diffraction data, and the Mn-disproportionation was determined from Seebeck-coefficient measurements as described earlier (Figure 7). The resulting cation distribution with the concentrations of Ni^{2+}, Mn^{2+}, and Mn^{3+} on tetrahedral positions, and those of Ni^{2+}, Mn^{3+}, and Mn^{4+} on octahedral sites, respectively, is shown as function of temperature in Figure 8. The concentration of Ni_B^{2+} is 0.87(3) at 55°C and decreases to about 0.70(1) at 900°C, resembling the reduction of ν with temperature. This is expected due to the high crystal field stabilization of Ni^{2+} ($3d^8$) in octahedral environment. Inversely, the Ni_A^{2+} is 0.13(3) at 55°C increasing to 0.30(1) at 900°C. The concentration of Mn_A^{3+} is practically zero at low temperature and starts to grow with temperature up to 600°C almost linearly. Above this temperature a steady state with a fixed concentration of 0.39(1) is reached remaining stable up to 900°C. In contrast, the concentration of Mn_A^{2+} is 0.86(3) at room temperature and decreases with temperature to 0.35(1) at 700°C. Simultaneously, the concentration of Mn_B^{4+} is 0.86(3) at room temperature and decreases with temperature to 0.31(1) at 900°C, demonstrating a high degree of Mn-disproportionation at low temperatures.

The concentration of Mn^{3+} on octahedral positions is governed by both, the degree of inversion ν and the disproportionation p. It varies between 0.27(3) near room temperature and 0.99(1) at 900°C (49% of octahedral Mn). As mentioned earlier, concentrations of Mn_B^{3+} larger than about 55%–65% are known to trigger cooperative JT distortions, for example, in Mn-rich $Ni_xMn_{3-x}O_4$,[51] or $MgMn_{2-x}Al_xO_4$.[52] In $NiMn_2O_4$, Mn_B^{3+} concentrations close to critical limit were found to exist at high temperatures only (Figure 8), but tetragonal distortions were not observed. To the best of our knowledge, nickel manganite has never been reported to be subject to tetragonal distortions at atmospheric conditions. However, Åsbrink et al.[53] reported a high pressure phase transition in $NiMn_2O_4$ at about 12 GPa to a tetragonally distorted spinel ($c/a < 1$), which was not reversible after decompression. They suggest that at sufficiently high pressure a completely inverse spinel with $\nu = 1$ and $p = 0$ appears, and the flattening of the cubic unit cell is caused by a large amount of Mn^{3+} on tetrahedral positions as well. Typically, elongated tetragonal spinel cells ($c/a > 1$) are reported for spinels with high Mn_B^{3+} concentrations and cooperative JT-distortions.[51,54]

Finally, the temperature-dependent cation distribution of $NiMn_2O_4$ (formula (2)) might be regarded as the result of cationic site or charge exchange processes. According to an approach used by Brabers et al.,[22] the cation exchange between the tetrahedral and octahedral sites is represented by the chemical equilibrium:

$$\begin{aligned} Ni_A^{2+} + Mn_B^{3+} + Mn_A^{3+} + Mn_B^{3+} \rightleftarrows Ni_B^{2+} \\ + Mn_A^{3+} + Mn_A^{2+} + Mn_B^{4+} \end{aligned} \quad (8)$$

Using the inversion parameter ν and the disproportionation parameter p from formula (2), the equilibrium constant K as follows:

$$\begin{aligned} K &= \frac{\nu(\nu - p)p^2}{(1-\nu)(2-\nu-p)(\nu-p)(2-\nu-p)} \\ &= e^{(-\Delta G_0/RT)} = e^{(\Delta S_0/R)} + e^{(-\Delta H_0/RT)} \end{aligned} \quad (9)$$

The variation of $\ln K$ versus $1000/T$ (Figure 9) shows the little variation of $\ln K$ between 55 and 300°C with a small slope, that is, small activation energy of 0.07 eV. In this low-temperature regime, the inversion ν is large and hardly changes with temperature, whereas easy electron exchange between Mn-ions allows for significant changes in the Mn ion distributions. In the intermediate temperature range (300–700°C), a larger activation energy of 0.55 eV is an indication of the simultaneous occurrence of two processes, that is, the exchange of cations between A- and B-sites (inversion ν) and change of Mn-ion distribution (disproportionation p). In the high temperature regime at $T > 700$°C, the activation energy is small again, as almost no change in the cation inversion is present.

Finally, the presented temperature-dependent cation distribution situation in $NiMn_2O_4$ (Figure 8) allows to identify a possible source of the observed aging behavior of the electrical resistivity of this NTC thermistor material. As discussed earlier, the Mn-disproportionation equilibrium involving exchange of electrons between Mn ions on A-sites or on B-sites only is operative at low temperatures. Already at $T < 150$°C, changes in the $[Mn^{4+}]/[Mn^{3+}]$ ratio on B-sites are observed (Figure 7), entailing changes in the concentrations of charge carriers and giving rise to changes in the resistivity and thus aging.

5 | CONCLUSION

We presented the results of a combined in situ neutron diffraction and thermopower study on $NiMn_2O_4$ in the temperature range from 55 to 900°C and shed light into the temperature-dependent cation distribution in this spinel oxide.

The degree of inversion ν, which involves the exchange of cations between A- and B-sites of the spinel lattice, is $\nu = 0.87(1)$ at 55°C as for an almost inverse spinel, and remains almost constant up to $T = 300$°C. As the

temperature increases, ν decreases and reaches $\nu = 0.71(1)$ at 800°C. No further change is observed up to the upper temperature limit of the measurements at 900°C.

The variation of the $[Mn_B^{4+}]/[Mn_B^{3+}]$ ratio and the disproportionation parameter p were calculated as function of temperature from the Seebeck coefficients using a modified Heikes formula. A degeneracy factor of 10/4 for Mn_B^{3+} was derived from the low-temperature Mn-disproportionation state of a quenched sample.

The results were combined with inversion parameters to derive a plausible model of the cation distribution in $NiMn_2O_4$ for the temperature range from 55 to 900°C. It is concluded that in the low-temperature range up to 300°C the cation inversion ν remains nearly constant, whereas the Mn-disproportionation situation changes significantly from $p = 0.86(3)$ at 55°C to 0.71(1) at 300°C. This might represent a major source of instability and may cause the observed aging of the resistivity of this NTC thermistor oxide. On further increase in temperature, the tendency toward disproportionation decreases and reaches $p = 0.32(1)$ at 800°C and remains almost unchanged up to 900°C. This corresponds to a high Mn^{3+} concentration on B-sites of 0.99(1). Nevertheless, this is below the critical concentration for cooperative tetragonal JT distortions, and the cubic structure of the spinel is maintained up to 900°C.

ACKNOWLEDGMENTS

The authors thank A. Bochmann (EAH Jena) for help in Seebeck coefficient measurements and Dr. Andreas Hoser (HZB, BER II) for the support on the instrument E9. Financial support from the Thuringian Ministry for Economy, Science and Digital Society—European Social Fund Thuringia, Germany (2015 FGR 0084) is acknowledged. The Helmholtz-Zentrum Berlin (HZB, BER II) is acknowledged for providing beam time.

Open access funding enabled and organized by Projekt DEAL.

ORCID

Jan Dinger https://orcid.org/0000-0002-0874-5387
Jörg Töpfer https://orcid.org/0000-0002-4022-4143

REFERENCES

1. Feteira A. Negative temperature coefficient resistance (NTCR) ceramic thermistors: an industrial perspective. J Am Ceram Soc. 2009;92(5):967–83.
2. Schmidt R, Basu A, Brinkman AW. Small polaron hopping in spinel manganates. Phys Rev B. 2005;72(11):115101.
3. Fritsch S, Sarrias J, Brieu JJ, Baudour JL, Snoeck E, Rousset A. Correlation between the structure, the microstructure and the electrical properties of nickel manganite negative temperature coefficient (NTC) thermistors. Solid State Ionics. 1998;109(3–4):229–37.
4. Groen WA, Metzmacher C, Huppertz P, Schuurman S. Aging of NTC ceramics in the system Mn-Ni-Fe-O. J Electroceram. 2001;7(2):77–87.
5. Fang D, Zheng C, Chen C, Winnubst AJA. Aging of nickel manganite NTC ceramics. J Electroceram. 2009;22(4):421–7.
6. Wickham DG. Solid-phase equilibria in the system NiO-Mn_2O_3-O_2. J Inorg Nucl Chem. 1964;26(8):1369–77.
7. Xiao-Xia T, Manthiram A, Goodenough JB. $NiMn_2O_4$ revisited. J Less-Common Met. 1989;156(1–2):357–68.
8. Feltz A, Töpfer J. Redoxreaktionen in kondensierten Oxidsystemen. X Bildung von Defektspinellen und Phasenbeziehungen im System $Ni_xMn_{3-x}O_4$. Z Anorg Allg Chem. 1989;576(1):71–80.
9. Sickafus KE, Wills JM, Grimes NW. Structure of spinel. J Am Ceram Soc. 1999;82(12):3279–92.
10. Sinha APB., Sanjana NR, Biswas AB. On the structure of some manganites. Acta Cryst. 1957;10(6):439–40.
11. Mănăilă R, Păuşescu P. Structural changes in $MgMn_2O_4$ at high temperatures. Physica Status Solidi B. 1965;9(2):385–94.
12. Dorris SE, Mason TO. Electrical properties and cation valencies in Mn_3O_4. J Am Ceram Soc. 1988;71(5):379–85.
13. Driessens F, Rieck GD. Phase equilibria in the system Zn-Mn-O in air. J Inorg Nucl Chem. 1966;28(8):1593–600.
14. Baltzer PK, White JG. Crystallographic and magnetic studies of the system $(NiFe_2O_4)_{1-x}+(NiMn_2O_4)_x$. J Appl Phys. 1958;29(3):445–7.
15. Boucher B, Buhl R, Perrin M. Etude cristallographique du manganite spinelle cubique $NiMn_2O_4$ par diffraction de neutrons. Acta Crystallogr B: Struct Sci. 1969;25(11):2326–33.
16. Larson EG, Arnott RJ, Wickham DG. Preparation, semiconduction and low-temperature magnetization of the system $Ni_{1-x}Mn_{2+x}O_4$. J Phys Chem Solids. 1962;23(12):1771–81.
17. Töpfer J, Feltz A, Gräf D, Hackl B, Raupach L, Weissbrodt P. Cation valencies and distribution in the spinels $NiMn_2O_4$ and $M_zNiMn_{2-z}O_4$ (M = Li, Cu) studied by XPS. Phys Status Solidi A. 1992;134(2):405–15.
18. Brabers VAM, van Setten FM, Knapen P. X-ray photoelectron spectroscopy study of the cation valencies in nickel manganite. J Solid State Chem. 1983;49(1):93–8.
19. Gillot B, Baudour JL, Bouree F, Metz R, Legros R, Rousset A. Ionic configuration and cation distribution in cubic nickel manganite spinels $Ni_xMn_{3-x}O_4$ (0.57<x<1) in relation with thermal histories. Solid State Ionics. 1992;58(1–2):155–61.
20. Sagua A, Lescano GM, Alonso JA, Martínez-Coronado R, Fernández-Díaz MT, Morán E. Neutron structural characterization, inversion degree and transport properties of $NiMn_2O_4$ spinel prepared by the hydroxide route. Mater Res Bull. 2012;47(6):1335–8.
21. Töpfer J, Feltz A, Dordor P, Doumerc JP. Thermopower analysis of substituted nickel manganite spinels. Mater Res Bull. 1994;29(3):225–32.
22. Brabers VAM, Terhell JCJM. Electrical conductivity and cation valencies in nickel manganite. Phys Status Solidi A. 1982;69(1):325–32.
23. Watanabe N, Nakayama H, Fukao K, Munakata F. Transport and x-ray photoelectron spectroscopy properties of $(Ni_{1-x}Cu_x)Mn_2O_4$ and $Ni(Mn_{2-y}Cu_y)O_4$. J Appl Phys. 2011;110(2):23519.

24. Dinger J, Reimann T, Ovodok E, Töpfer J. Cation distribution in NiMn2O4 spinel probed by high temperature thermopower measurements. J Alloys Compd. 2021;865:158909.
25. Franz A, Hoser A. E9: the fine resolution powder diffractometer (FIREPOD) at BER II. JLSRF. 2017;3(3):103.
26. Feltz A, Töpfer J, Schirrmeister F. Conductivity data and preparation routes for $NiMn_2O_4$ thermistor ceramics. J Eur Ceram Soc. 1992;9(3):187–91.
27. Jung J, Töpfer J, Mürbe J, Feltz A. Microstructure and phase development in NiMn2O4 spinel ceramics during isothermal sintering. J Eur Ceram Soc. 1990;6(6):351–9.
28. Koester L, Rauch H, Seymann E. Neutron scattering lengths: a survey of experimental data and methods. At Data Nucl Data Tables. 1991;49(1):65–120.
29. Baudour JL, Bouree F, Fremy MA, Legros R, Rousset A, Gillot B. Cation distribution and oxidation states in nickel manganites $NiMn_2O_4$ and $Ni_{0.8}Mn_{2.2}O_4$ from powder neutron diffraction. Physica B. 1992;180–181:97–9.
30. Brabers VAM. Ionic ordering and infrared spectra of some II-IV spinels. Phys Status Solidi A. 1972;12(2):629–36.
31. Ferreira RA, Tedesco JC, Birk JO, Kalceff W, Yokaichiya F, Rasmussen N, et al. Ferrimagnetism and spin excitation in a Ni–Mn partially inverted spinel prepared using a modified polymeric precursor method. Mater Chem Phys. 2014;146(1–2):58–64.
32. Islam MS, Catlow CRA. Structural and electronic properties of NiMn2O4. J Phys Chem Solids. 1988;49(2):119–23.
33. Kshirsagar ST. Electrical and crystallographic studies of the system $Cu_xNi_{1-x}Mn_2O_4$. J Phys Soc Jpn. 1969;27(5):1164–70.
34. Laberty C, Verelst M, Lecante P, Alphonse P, Mosset A, Rousset A. A wide angle x-ray scattering (WAXS) study of nonstoichiometric nickel manganite spinels $NiMn_2\square_{3\delta/4}O_{4+\delta}$. J Solid State Chem. 1997;129(2):271–6.
35. Krupička S, Novák P. Chapter 4: Oxide spinels. In: Handbook of ferromagnetic materials. vol. 3. Amsterdam, Netherlands: Elsevier; 1982. p. 189–304.
36. Shannon RD. Revised effective ionic radii and systematic studies of interatomic distances in halides and chalcogenides. Acta Crystallogr A. 1976;32(5):751–67.
37. Heikes RR, Ure RW Jr. Classical and irreversible thermodynamic treatment of thermoelectricity. In: *Thermoelectricity: Science and Engineering*. Interscience Publ., New York-London; 1961. p.-7-17.
38. Wu CC, Mason TO. Thermopower measurement of cation distribution in magnetite. J Am Ceram Soc. 1981;64(9):520–2.
39. Chaikin PM, Beni G. Thermopower in the correlated hopping regime. Phys Rev B. 1976;13(2):647–51.
40. Doumerc J-P. Thermoelectric power for carriers in localized states: a generalization of Heikes and Chaikin-Beni formulae. J Solid State Chem. 1994;109(2):419–20.
41. March DB, Paris PE. Theory of the Seebeck coefficient in $LaCrO_3$ and related perovskite systems. Phys Rev B. 1996;54(11):7720.
42. Koshibae W, Maekawa S. Effects of spin and orbital degeneracy on the thermopower of strongly correlated systems. Phys Rev Lett. 2001;87(23):236603.
43. Koshibae W, Tsutsui K, Maekawa S. Thermopower in cobalt oxides. Phys Rev B. 2000;62(11):6869–72.
44. Kobayashi W, Terasaki I, Mikami M, Funahashi R, Nomura T, Katsufuji T. Universal charge transport of the Mn oxides in the high temperature limit. J Appl Phys. 2004;95(11):6825–7.
45. Töpfer J, Feltz A. Investigations on electronically conducting oxide systems XXIV[1]: preparation and electrical properties of the spinel series $Cu_zNiMn_{2-z}O_4$. Solid State Ionics. 1993;59(3–4):249–56.
46. Sturge MD. The Jahn-Teller effect in solids. Amsterdam, Netherlands: Elsevier; 1968.
47. Buhl R. Manganites spinelles purs d'elements de transition preparations et structures cristallographiques. J Phys Chem Solids. 1969;30(4):805–12.
48. Wickham DG. The chemical composition of spinels in the system Fe_3O_4-Mn_3O_4. J Inorg Nucl Chem. 1969;31(2):313–20.
49. Wickham DG, Croft WJ. Crystallographic and magnetic properties of several spinels containing trivalent ja-1044 manganese. J Phys Chem Solids. 1958;7(4):351–60.
50. Dorris SE, Mason TO. Electrical properties and cation valencies in Mn_3O_4. J Am Ceram Soc. 1988;71(5):379–85.
51. Gillot B, Kharroubi M, Metz R, Legros R, Rousset A. Electrical properties and cationic distribution in cubic nickel manganite spinels $Ni_xMn_{3-x}O_4$, $0.57<x<1$. Solid State Ionics. 1991;44(3–4):275–80.
52. Bosi F, Halenius U, Skogby H. Crystal chemistry of the MgAl2O4-MgMn2O4-MnMn2O4 system: analysis of structural distortion in spinel- and hausmannite-type structures. Am Mineral. 2010;95(4):602–7.
53. Åsbrink S, Waśkowska A, Olsen JS, Gerward L. High-pressure phase of the cubic spinel $NiMn_2O_4$. Phys Rev B. 1998;57(9):4972–4.
54. Martín de Vidales JL, Rojas RM, Vila E, García-Martínez O. Low temperature synthesis of tetragonal nickel manganite spinels: thermal behaviour and reactivity. Mater Res Bull. 1994;29(11):1163–73.

How to cite this article: Dinger J, Friedrich T, Reimann T, Töpfer J. $NiMn_2O_4$ revisited: Temperature-dependent cation distribution from in situ neutron diffraction and thermopower studies. J Am Ceram Soc. 2022;1–14.
https://doi.org/10.1111/jace.18865